

Crystal chemistry of double-ring silicates: Structural, chemical, and optical variation in osumilites

THOMAS ARMBRUSTER

Laboratorium für chemische und mineralogische Kristallographie, Universität Bern, Freiestr. 3, CH-3012 Bern, Switzerland

ROLAND OBERHÄNSLI

Laboratorium für Mikroröntgenspektroskopie, Universität Bern, Baltzerstr. 1, CH-3012 Bern, Switzerland

ABSTRACT

Crystal structures including site occupancies of eight natural osumilites (space group $P6/mcc$, crystal-chemical formula: $CA_2(T2)_3(T1)_{12}O_{30}$) from regional metamorphic rocks, from contact-metamorphosed xenoliths, and from igneous rocks were refined from X-ray single-crystal data. There is a strong positive correlation between the size of the cation (Mg, Fe, Al) in octahedral coordination (A site) and the length of the a axis. However, the size increase of the AO_6 octahedron is not reflected in the size of the edge-sharing tetrahedra. The 12-coordinated C site, located between two double rings of (Si,Al) O_4 tetrahedra (T1), is mainly occupied by K. When osumilite contains octahedral Al, a high concentration of vacancies is observed on the C site: ${}^{VI}Al^{3+} + {}^{XII}vacancy = {}^{VI}(Mg, Fe^{2+}) + {}^{XII}(K, Na)$. In all samples, T2 is predominantly occupied by Al with minor Fe and Mg.

Osumilites rich in octahedral Mg possess the highest birefringence and are optically positive. With increasing Fe content on the A site, ω increases more strongly than ϵ , thus reducing the birefringence. Linear-regression analyses of refractive indices versus octahedral (Fe + Mn + Ti) predict osumilites with more than 90% (Fe + Mn + Ti) on the A site to be optically negative.

INTRODUCTION

Osumilite (Miyashiro, 1956), with the crystal-chemical formula ${}^{XII}C{}^{VI}A_2{}^{IV}(T2)_3{}^{IV}(T1)_{12}O_{30}$ (Forbes et al., 1972), crystallizes in the space group $P6/mcc$ and belongs to the group of double-ring silicates. T1 tetrahedra form six-membered double rings and are predominantly occupied by Si and to a lesser extent by Al. T2 tetrahedra are occupied by Al with little Fe and Mg (Hesse and Seifert, 1982). Octahedra (A sites) are occupied by Mg and Fe and form edge-sharing 12-membered rings together with T2 tetrahedra (Fig. 1). Alternating T1 double rings (Fig. 2) and T2/A rings are stacked above each other, thus forming continuous channels running parallel to the c axis. These channels are plugged by K occupying the C position, situated between two sets of double rings. In double-ring silicates, two additional atomic positions are known, ${}^{XVIII}D$ in the center of a double-ring unit and ${}^{IX}B$ at $1/3, 2/3, 0$ but slightly displaced from it along the threefold axis ($1/3, 2/3, z$) (Forbes et al., 1972). However, both sites are assumed to be vacant in osumilites.

Although osumilite was considered a rare mineral 10 years ago, today, 24 natural occurrences are known (Schreyer et al., 1986) ranging from "dry"² granulite-facies metamorphic assemblages, contact-metamorphosed

sedimentary rocks, xenoliths in volcanic rocks, and buchites to volcanic formations.

The stability of synthetic K-Mg-bearing osumilite has been experimentally established to lie between ca. 700 °C and 950 °C at H_2O pressures below 0.8 kbar ($P_{H_2O} = P_{tot}$) (Olesch and Seifert, 1981). When formed at higher pressures, this mineral suggests a very low f_{H_2O} .

Although a large number of osumilite occurrences have been reported and the chemical variation of this mineral is well documented (e.g., Grew, 1982; Schreyer et al., 1983), several questions remain unanswered. EXAFS studies (Waychunas et al., 1986) confirm Mössbauer measurements (Goldman and Rossman, 1978) indicating that an osumilite from Nain, Labrador, bears Fe^{2+} on the A octahedral site and on an additional highly disordered site (channel site). Single-crystal X-ray studies on a crystal from the same locality (Hesse and Seifert, 1982), however, yielded Fe^{2+} in the A octahedron and T2, but no evidence for channel Fe^{2+} was found. In addition, the relationship between unit-cell dimensions and chemistry is not understood, leading to the question: how does this condensed tetrahedral framework structure accommodate chemical variations?

When Miyashiro (1956) first described osumilite, he noted that this mineral was previously considered to be cordierite. Indeed, Fe-bearing osumilites reveal striking dichroism: blue parallel to O and colorless to brown parallel to E . However, most osumilites are uniaxial posi-

¹ Roman superscripts denote coordination numbers.

² In this context, "dry" only means that a_{H_2O} is very low or that a_{CO_2} , a_{CH_4} , etc. are high—not that a fluid phase was absent.

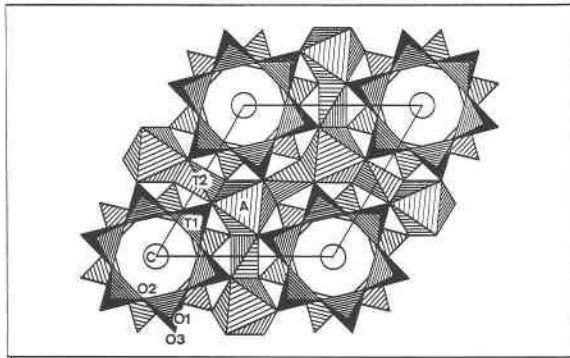


Fig. 1. The osumilite structure projected along the *c* axis. O2 oxygen atoms connect T1 tetrahedra to six-membered rings and O1 oxygens link the single rings to form double rings. In this projection, the double rings appear only as single rings because the doubling is caused by a mirror plane perpendicular to *c*. The cage position C is situated between two sets of double rings. The T2 and A positions, forming twelve-membered rings of edge-sharing octahedra (A) and tetrahedra (T2), are at the same height $c/4$ as C.

tive, whereas most hexagonal cordierites (indialites) or pseudo-hexagonal cordierites (yielding broadened hexagonal X-ray powder patterns) are optically negative. Recently, Schreyer et al. (1983) reported optically negative as well as optically positive osumilites from the Eifel district (F.R.G.). Some questions remain, therefore, concerning the structural and/or chemical reason for optically positive and negative osumilites. In addition, some metamorphic osumilites are optically biaxial ($2V_z$ up to 40°), and Goldman and Rossman (1978) have argued that the irregular distribution of channel Fe^{2+} is responsible for this anomalous behavior.

In the present paper, we report single-crystal X-ray structure refinements, optical measurements, and electron-microprobe analyses of a series of eight osumilites from various localities.

SAMPLE DESCRIPTION AND OSUMILITE COMPOSITION

Two osumilites from metamorphic terranes, two from contact metamorphosed xenoliths, and four of volcanic origin were investigated.

Samples from metamorphic terranes

The "Antarctica" (NMBE-B5561) osumilite originates from Mount Riiser-Larsen, Enderby Land, Antarctica. The locality is shown in Figure 1 of Grew (1982). Sample 2337K of Grew (1982) contains the assemblage quartz, osumilite, orthopyroxene, K-feldspar, biotite, and zircon. This sample has been chosen from among other samples from Mount Riiser-Larsen because of its high Mg and low Fe content (Table 1).

The Norwegian sample (NMBE-B5562) was collected by us in the area of Vikeså where banded, migmatitic metapelitic rocks occur within the charnockitic Precam-

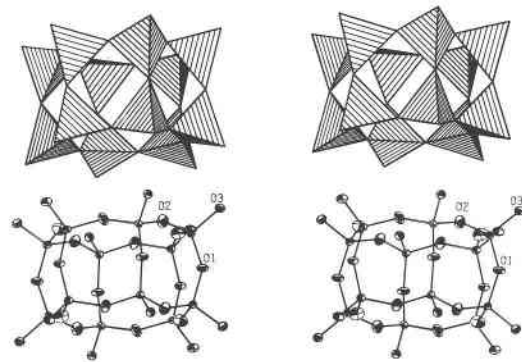


Fig. 2. Stereo pairs of double-ring units seen edgewise. Upper row, coordination tetrahedra model; lower row, bond-stick model with thermal ellipsoids using the data of the Eifel B93 sample.

brian basement (Maijer et al., 1977), which was contact-metamorphosed by neighboring anorthosites.

In contrast to all other osumilites described in this paper, the Norwegian osumilite exhibits an unusual pink color. Because of the abundance of osumilite, this rock shows a bluish-purple hue. Osumilite coexists with quartz, mesoperthite, plagioclase, orthopyroxene, garnet, biotite, and green spinel as well as magnetite and ilmenite. Where altered, osumilite decomposes to symplectitic aggregates of quartz, K-feldspar, and cordierite. Along fractures with access to fluids, both K-feldspar and osumilite alter to sericite (presumably owing to the availability of H_2O).

Contact metamorphosed xenoliths

Two different types of osumilites from the volcanic Eifel district (F.R.G.) were investigated. The sample "Eifel B93" comprises thin, tabular, dark blue plates grown in vesicles of contact-metamorphosed xenoliths from the Bellerberg near Mayen (F.R.G.). Crystals from the same hand specimen were previously described and analyzed by Schreyer et al. (1983, their no. BIII).

The second Eifel osumilite occurs together with Mg-rich cordierite on the surface of contact-metamorphosed xenoliths from Nickenich (F.R.G.) (NMBE-B3431). The hexagonal prismatic crystals appear macroscopically dark blue to gray owing to magnetite inclusions. Microscopically, this osumilite is colorless and transparent.

Volcanic samples

The osumilite labeled "Sardinia" (NMBE-B5558) originates from Cava Funtanafigu, a rhyolite quarry between Cagliari and Oristano on Sardinia, Italy (Hochleitner, 1982). The dark blue, hexagonal, prismatic-tabular crystals grow within the thin fissures that run parallel to the fluidal texture of the rhyolite.

The "Oregon" sample (NMBE-A8491) comprises hexagonal prismatic crystals grown on a fissure within a rhyolite from North Sister Mountain, Lane County, Oregon, U.S.A. Specimens from Obsidian Cliffs, near McKenzie Pass, Oregon (probably the same locality or one close to North Sister Mountain), were described by

Olsen and Bunch (1970) and Goldman and Rossman (1978).

Two samples from Japan were studied—one from Shimizu, Kagoshima (NMBE-A8458), with regular dark blue hexagonal prisms covering a rhyolite fissure and the other (NMBE-B5560) from a "plagiolarite" from Hayasaki, Sakkabira, where dark blue osumilite prisms are mostly enclosed in tiny vesicles (Miyashiro, 1956).

MICROPROBE ANALYSES

For this work, single crystals were separated from hand specimens ca. 1 in. (2.5 cm) in diameter. Microprobe analyses and single-crystal measurements were carried out on different grains, for two reasons: (1) Osumilites from volcanic rocks and from xenoliths are often strongly zoned with respect to Fe and Mg. Thus, even sets of two-dimensional point analyses collected on the same grain as used for the single-crystal experiments are hardly representative of the three-dimensional crystal. (2) Small crystals used for X-ray structure work are easily lost during grinding and polishing for the preparation of microprobe mounts. Thus, because only one small crystal from Nickenich (Eifel, F.R.G.) was available, a microprobe analysis was not performed on it. All analyses presented in Table 1 are mean values of measurements collected on several grains.

Mineral compositions were determined using an automated, combined wavelength-dispersive (WDS) and energy-dispersive (EDS) microprobe system (ARL-SEM-Q and Tracor Northern 2000). An acceleration potential of 15 kV, a sample current of 20 nA measured on brass, and a beam size of approximately 3 μm were used. Natural and synthetic oxides and silicates were used as standard materials. The raw data were corrected on line for drift, deadtime, and background. Matrix corrections were calculated using a ZAF correction procedure.

OPTICAL AND X-RAY EXPERIMENTS

All hand-picked osumilite crystals were mounted on glass fibers and inspected in oil immersion under a spindle stage-equipped polarizing microscope (Bloss, 1981) to check for intergrowth, inclusions, and twinning. If possible, refractive indices were refined for 25 °C and 589.3 nm from double variation measurements (wavelength, temperature). The crystals from the Eifel district, however, contained either numerous magnetite inclusions (Nickenich sample) or a reaction coating on the surface (Bellerberg sample); thus, refractive-index measurements were not performed.³ Fe-rich crystals, e.g., from Japan, Oregon, Sardinia, and Eifel (Bellerberg), show an intense and broad absorption band at ca. 650 nm (Goldman and Rossman, 1978) for light polarized parallel to (001) (i.e., \parallel O). In this direction, these crystals appear dark blue, which makes refractive-index measurement more difficult and inaccurate.

³ X-ray work is not significantly influenced by the low concentration of impurities.

TABLE 1. Average composition of osumilites

	Antarctica <i>n</i> = 14	Norway <i>n</i> = 8	Eifel B93 <i>n</i> = 4	Japan Shimizu <i>n</i> = 4	Japan Haysaki <i>n</i> = 4	Sardinia <i>n</i> = 3	Oregon <i>n</i> = 4
SiO ₂	62.75	61.95	59.45	60.97	60.51	60.97	60.01
TiO ₂	0.08	0.00	0.06	0.05	0.04	0.04	0.05
Al ₂ O ₃	21.65	21.86	24.56	21.35	21.60	21.66	21.46
FeO	0.94	3.75	12.85	9.06	9.27	9.34	8.96
MnO	0.00	0.07	0.52	1.06	0.99	0.46	1.02
MgO	9.07	6.87	0.41	3.15	3.05	3.47	3.27
CaO	0.10	0.00	0.00	0.09	0.00	0.07	0.06
BaO	0.00	0.00	0.01	0.02	0.04	0.00	0.05
Na ₂ O	0.28	0.42	0.10	0.66	0.67	0.68	0.06
K ₂ O	4.60	4.33	1.59	3.45	3.46	3.44	3.32
Total	99.47	99.25	99.55	99.86	99.63	99.97	98.20
Osumilite formulae based on 30 oxygen atoms							
Si	10.37	10.37	10.17	10.40	10.36	10.35	10.38
Al	1.63	1.63	1.83	1.60	1.64	1.65	1.62
Σ	12.00	12.00	12.00	12.00	12.00	12.00	12.00
Al	2.59	2.69	3.13	2.69	2.72	2.69	2.76
Fe ²⁺	0.13	0.53	1.84	1.29	1.33	1.33	1.30
Mn ²⁺	0.00	0.01	0.08	0.15	0.14	0.07	0.15
Mg	2.23	1.72	0.11	0.80	0.78	0.88	0.84
Ti ⁴⁺	0.01	0.00	0.01	0.01	0.01	0.01	0.01
Σ	4.96	4.95	5.17	4.95	4.98	4.98	5.06
Ca	0.02	0.00	0.00	0.02	0.00	0.01	0.00
Ba	0.00	0.00	0.00	0.00	0.00	0.00	0.00
Na	0.09	0.14	0.03	0.22	0.22	0.22	0.02
K	0.97	0.93	0.35	0.75	0.76	0.75	0.73
Σ	1.08	1.07	0.38	0.99	0.98	0.98	0.75

In the case of optical biaxiality, the optic axial angle was calculated by the computer program EXCALIBR (Bloss, 1981) from an extinction data set obtained under crossed nicols. Significant biaxiality ($2V_z \geq 10^\circ$) was found in osumilites from Norway with $2V_z$ up to 45° and from Hayasaki, Japan, with $2V_z$ up to 28° .

Selected crystals or crystal fragments were subsequently transferred to a precession camera for space group ($P6/mcc$) confirmation. During this procedure, it was found that most tabular osumilites from Bellerberg were twinned perpendicular to the (001) plane. Within 001 twin precession photographs, several sets of spots are common to both individuals of the twin, e.g., $2hhl$, $h4hl$, $7h0l$, $9hhl$, $5h6hl$, $3h5hl$, $7h7hl$. This twin type with a parallel optic axis is not detectable by optical methods.

Intensity data of untwinned crystals were collected on an Enraf-Nonius CAD4 single-crystal X-ray diffractometer (graphite-monochromatized $\text{MoK}\alpha$ radiation) with an omega scan mode. Cell parameters were determined from least-squares refinements of 24 automatically centered reflections (0012, 800, 444, 8014, and their symmetry equivalents). Intensities of all reflections with $h \geq k$ and h, k, l positive were collected up to $\theta = 30^\circ$. Reflections for which a prescan determined $[\sigma(I)/I] \geq 1$ were flagged as weak. The final scan speed was calculated from the prescan in order to obtain $[\sigma(I)/I] = 0.03$. Reflections of the type hhl and $h0l$ with $l \neq 2n$ were considered as systematically absent and rejected. For all crystals, the reflection 0015 revealed low but significant intensity up to 35 times its estimated standard deviation and is inconsistent with $P6/mcc$. However, one low-intensity forbidden reflection

TABLE 2. Details of X-ray data collection, cell dimensions, refractive indices, and crystal size

Sample name	Reflections (measured) (contribut.)	R R_w (%)	a_0 c_0 (Å)	ω ϵ	Crystal size (mm)	Absorption extinction correction
Antarctica	648	2.1	10.086(3)	1.5365	0.07 × 0.13 × 0.13	
	491	3.3	14.325(4)	1.5446		
Norway	649	5.6	10.104(2)	1.539	0.07 × 0.07 × 0.13	A
	430	6.9	14.306(3)	1.546		
Labrador*		3.3	10.126(2)	1.5406		
	590		14.319(3)	1.5473		
Eifel— B93**	646	2.2	10.071(2)	1.565	0.05 × 0.15 × 0.23	
	348	2.6	14.303(4)	1.563		
Eifel— Nickenich	646	2.2	10.078(2)		0.10 × 0.15 × 0.20	A
Japan— Shimizu	513	3.5	14.319(2)		0.28 × 0.35 × 0.35	A E
	653	2.0	10.145(2)			
Japan— Hayasaki	599	3.4	14.289(2)		0.10 × 0.15 × 0.30	A
	655	2.1	10.150(2)	1.5515		
Sardinia	505	3.0	14.286(3)	1.5538		
	653	2.2	10.127(3)	1.5457		
Oregon	499	3.2	14.288(4)	1.5500	0.12 × 0.25 × 0.25	A E
	625	2.0	10.137(2)	1.548		
	539	3.3	14.308(3)	1.5530		

* Crystal structure, Hesse and Seifert (1982); refractive indices, Berg and Wheeler (1976).

** Refractive indices from Schreyer et al. (1983).

was considered insufficient for choice of another hexagonal space group. For uneven-dimensioned crystals, an empirical absorption correction (psi scans) was applied (marked "A" in Table 2).

Data reduction, including background and Lorentz-polarization corrections, was carried out with the SDP program system (Enraf Nonius, 1983).

Reflections allowed under $P6/mcc$ symmetry were employed for the refinements of the structure using the start values of Hesse and Seifert (1982) with the program system PROMETHEUS (Zucker et al., 1983). Structure factors were weighted on the basis of counting statistics ($w = 1/\sigma^2$), applying a $6\sigma(F_{\text{obs}})$ cutoff. Neutral-atom scattering factors and real as well as imaginary parts of the anomalous dispersion corrections were used. If comparison between observed and calculated structure factors indicated extinction, an isotropic extinction correction (Becker and Coppens, 1974) was applied (marked "E" in Table 2). Observed and calculated structure factors are compiled in Table 3.⁴ In addition to positional and displacement parameters (Table 4), site occupancies on the C site (allowing for K and vacancies), on the A site (allowing for Mg and Fe), and on the T2 site (allowing for Al and Fe) were refined (Table 5).

Compared to all other osumilite refinements, the crystal from Norway yielded by far the highest R values (Table 2). In addition, very wide scans were necessary to cover the broad reflections. As noted above, this crystal was also biaxial, and most osumilite crystals from the

same hand specimen revealed symplectitic intergrowths (K-feldspar-cordierite-quartz). Most likely, the Norway individual used for crystal-structure work also contained these submicroscopic symplectitic domains. Difference-Fourier maps for this crystal did not indicate peaks higher than $\pm 1 e/\text{\AA}^3$ and were not significantly different from the maps of other osumilites ($\pm 0.5 e/\text{\AA}^3$).

RESULTS

Table 6 summarizes selected atom-atom distances and angles. All statistical tests on osumilite distances and angles were performed on crystals described in this paper and the Nain, Labrador, osumilite of Hesse and Seifert (1982).

THE A OCTAHEDRON

The a dimension of the unit cell shows a strong positive correlation with the size of the atom on the A site reflected by the A-O distance (Fig. 3). A similar effect has been observed in the structurally closely related cordierites (Selkregg and Bloss, 1980; Armbruster, 1985) and beryls (Bakakin et al., 1970). In cordierites the c -axis length decreases with increasing M-O distance (M in cordierite is an equivalent position to A in osumilite). This decrease is also noticed in osumilites; though, the correlation is less pronounced ($R^2 = 33\%$). Introduction of the C-O or T2-O distances as additional independent parameters did not improve the correlation. However, the correlation increased ($R^2 = 62\%$) if a second-order model was assumed with A-O as variable parameter, or if a first-order model was chosen and the specimen Eifel B93 was excluded ($R^2 = 63\%$).

One might assume that the A-O distance is prescribed by the degree of Fe ↔ Mg substitution. This correlation

⁴ A copy of Table 3 may be ordered as Document AM-88-373 from the Business Office, Mineralogical Society of America, 1625 I Street, N.W., Suite 414, Washington, D.C. 20006, U.S.A. Please remit \$5.00 in advance for the microfiche.

TABLE 4. Fractional atomic coordinates, displacement parameters, and site occupancies (*P*)

	Antarctica	Norway	Eifel B93	Eifel Nickenich	Japan Shimizu	Japan Hayasaki	Sardinia	Oregon	
C	<i>P</i> (K)	0.91(1)	0.90(1)	0.48(1)	0.69(1)	0.74(1)	0.76(1)	0.75(1)	0.69(1)
	<i>x</i>	0	0	0	0	0	0	0	0
	<i>y</i>	0	0	0	0	0	0	0	0
	<i>z</i>	1/4	1/4	1/4	1/4	1/4	1/4	1/4	1/4
	<i>B</i> _{eq}	2.37(3)	2.59(9)	2.50(9)	2.69(4)	2.78(2)	2.80(3)	2.89(4)	2.68(3)
	<i>U</i> ₁₁	0.0255(7)	0.029(3)	0.029(3)	0.030(1)	0.0307(8)	0.031(1)	0.032(1)	0.030(1)
	<i>U</i> ₂₂	0.0255	0.029	0.029	0.030	0.0307	0.031	0.032	0.030
	<i>U</i> ₃₃	0.031(1)	0.031(4)	0.028(4)	0.033(2)	0.034(1)	0.034(1)	0.035(2)	0.032(1)
	<i>U</i> ₁₂	0.0127	0.014	0.014	0.015	0.015	0.016	0.016	0.016
A	<i>P</i> (Fe)	0.01(1)	0.16(2)	0.67(1)	0.01(1)	0.56(1)	0.58(1)	0.41(1)	0.51(1)
	<i>x</i>	1/3	1/3	1/3	1/3	1/3	1/3	1/3	1/3
	<i>y</i>	2/3	2/3	2/3	2/3	2/3	2/3	2/3	2/3
	<i>z</i>	1/4	1/4	1/4	1/4	1/4	1/4	1/4	1/4
	<i>B</i> _{eq}	0.61(2)	0.67(5)	0.69(2)	0.58(2)	0.699(7)	0.66(1)	0.66(1)	0.734(8)
	<i>U</i> ₁₁	0.0054(6)	0.007(1)	0.0068(5)	0.0053(6)	0.0072(2)	0.0066(3)	0.0068(3)	0.0073(3)
	<i>U</i> ₂₂	0.0054	0.007	0.0068	0.0053	0.0072	0.0066	0.0068	0.0073
	<i>U</i> ₃₃	0.0107(8)	0.009(2)	0.0105(7)	0.0098(8)	0.0099(3)	0.0097(4)	0.0090(5)	0.0100(3)
	<i>U</i> ₁₂	0.0027	0.0035	0.0034	0.0027	0.0036	0.0033	0.0034	0.0038
T1	(Si,Al)								
	<i>x</i>	0.24821(6)	0.2501(2)	0.2466(1)	0.24734(6)	0.24750(4)	0.24738(6)	0.24725(7)	0.24775(6)
	<i>y</i>	0.35359(6)	0.3554(2)	0.3538(1)	0.35333(7)	0.35074(5)	0.35055(6)	0.35136(7)	0.35119(6)
	<i>z</i>	0.39206(4)	0.3921(1)	0.39217(5)	0.39204(4)	0.39191(3)	0.39187(4)	0.39189(4)	0.39208(3)
	<i>B</i> _{eq}	0.756(9)	0.72(2)	1.03(1)	0.813(9)	0.769(8)	0.758(9)	0.80(1)	0.859(9)
	<i>U</i> ₁₁	0.0086(3)	0.0084(8)	0.0113(5)	0.0094(3)	0.0088(2)	0.0088(3)	0.0093(3)	0.0099(3)
	<i>U</i> ₂₂	0.0099(3)	0.0100(8)	0.0137(5)	0.0107(3)	0.0105(2)	0.0105(3)	0.0115(3)	0.0118(3)
	<i>U</i> ₃₃	0.0077(3)	0.0058(6)	0.0100(3)	0.0080(3)	0.0068(2)	0.0069(2)	0.0068(3)	0.0077(2)
	<i>U</i> ₁₂	0.0055(2)	0.0046(6)	0.0063(4)	0.0060(2)	0.0055(2)	0.0056(2)	0.0060(2)	0.0062(2)
	<i>U</i> ₁₃	0.0015(2)	0.0010(6)	0.0018(4)	0.0016(2)	0.0013(1)	0.0014(2)	0.0014(2)	0.0012(2)
	<i>U</i> ₂₃	0.0017(2)	0.0010(6)	0.0006(5)	0.0017(2)	0.0013(1)	0.0014(2)	0.0015(2)	0.0011(2)
T2	<i>P</i> (Fe)	0.01(1)	0.03(1)	0.08(1)	0.08(1)	0.06(1)	0.07(1)	0.06(1)	0.06(1)
	<i>x</i>	1/2	1/2	1/2	1/2	1/2	1/2	1/2	1/2
	<i>y</i>	1/2	1/2	1/2	1/2	1/2	1/2	1/2	1/2
	<i>z</i>	1/4	1/4	1/4	1/4	1/4	1/4	1/4	1/4
	<i>B</i> _{eq}	0.70(1)	0.75(4)	1.91(3)	1.15(1)	0.753(8)	0.77(1)	0.82(1)	0.99(1)
	<i>U</i> ₁₁	0.0091(5)	0.010(1)	0.029(1)	0.0163(5)	0.0102(3)	0.0105(5)	0.0116(4)	0.0139(4)
	<i>U</i> ₂₂	0.0091	0.010	0.029	0.0163	0.0102	0.0105	0.0116	0.0139
	<i>U</i> ₃₃	0.0068(5)	0.006(1)	0.0117(8)	0.0091(5)	0.0063(3)	0.0069(5)	0.0061(5)	0.0079(4)
	<i>U</i> ₁₂	0.0072(5)	0.007(1)	0.026(1)	0.0137(5)	0.0073(5)	0.0080(4)	0.0089(5)	0.0107(4)
O1	<i>x</i>	0.1229(3)	0.1238(8)	0.1252(4)	0.1237(3)	0.1198(2)	0.1198(3)	0.1207(3)	0.1204(3)
	<i>y</i>	0.4079(3)	0.4090(7)	0.4085(4)	0.4071(3)	0.4044(2)	0.4041(3)	0.4049(3)	0.4061(3)
	<i>z</i>	0	0	0	0	0	0	0	0
	<i>B</i> _{eq}	1.63(4)	1.6(1)	1.86(6)	1.71(4)	1.75(3)	1.66(4)	1.69(5)	1.74(4)
	<i>U</i> ₁₁	0.026(1)	0.025(4)	0.026(2)	0.027(1)	0.0278(9)	0.027(1)	0.027(1)	0.026(1)
	<i>U</i> ₂₂	0.020(1)	0.017(3)	0.024(2)	0.022(1)	0.0214(9)	0.019(1)	0.021(1)	0.023(1)
	<i>U</i> ₃₃	0.0072(9)	0.009(2)	0.010(1)	0.0079(9)	0.0086(6)	0.0080(9)	0.007(1)	0.0081(8)
	<i>U</i> ₁₂	0.011(1)	0.004(3)	0.010(2)	0.012(1)	0.0118(7)	0.010(1)	0.010(1)	0.012(1)
O2	<i>x</i>	0.2166(2)	0.2196(6)	0.2208(4)	0.2176(2)	0.2145(2)	0.2144(2)	0.2152(2)	0.2159(2)
	<i>y</i>	0.2847(2)	0.2911(6)	0.2878(3)	0.2851(2)	0.2833(2)	0.2830(2)	0.2833(2)	0.2851(2)
	<i>z</i>	0.1320(1)	0.1327(3)	0.1323(2)	0.1318(1)	0.13159(9)	0.1319(1)	0.1316(1)	0.1313(1)
	<i>B</i> _{eq}	2.35(3)	2.5(1)	2.69(5)	2.34(3)	2.28(2)	2.30(3)	2.33(4)	2.31(3)
	<i>U</i> ₁₁	0.028(1)	0.029(3)	0.032(2)	0.027(1)	0.0261(7)	0.025(1)	0.027(1)	0.0260(9)
	<i>U</i> ₂₂	0.035(1)	0.043(3)	0.036(2)	0.033(1)	0.0336(7)	0.035(1)	0.035(2)	0.034(1)
	<i>U</i> ₃₃	0.0228(9)	0.021(2)	0.029(1)	0.0245(9)	0.0228(6)	0.0233(9)	0.0223(9)	0.0236(8)
	<i>U</i> ₁₂	0.0244(9)	0.030(3)	0.027(1)	0.0238(9)	0.0233(6)	0.0239(9)	0.024(1)	0.0232(8)
	<i>U</i> ₁₃	-0.0017(8)	-0.005(2)	0.006(1)	-0.0001(8)	-0.0011(5)	-0.0011(7)	-0.0015(8)	-0.0004(7)
	<i>U</i> ₂₃	-0.0048(8)	-0.004(2)	0.001(1)	-0.0025(8)	-0.0036(6)	-0.0036(7)	-0.0035(8)	-0.0018(7)
O3	<i>x</i>	0.1398(2)	0.1383(5)	0.1416(3)	0.1410(2)	0.1373(1)	0.1371(2)	0.1383(2)	0.1375(2)
	<i>y</i>	0.4934(2)	0.4936(5)	0.4949(3)	0.4937(2)	0.4904(1)	0.4905(2)	0.4913(2)	0.4909(2)
	<i>z</i>	0.1790(1)	0.1789(3)	0.1790(1)	0.1787(1)	0.17887(8)	0.1789(1)	0.1787(1)	0.17918(9)
	<i>B</i> _{eq}	1.18(2)	1.25(6)	1.68(4)	1.27(2)	1.32(2)	1.30(2)	1.34(3)	1.34(2)
	<i>U</i> ₁₁	0.0138(7)	0.016(2)	0.022(1)	0.0153(7)	0.0164(5)	0.0159(7)	0.0163(8)	0.0160(7)
	<i>U</i> ₂₂	0.0155(7)	0.016(2)	0.023(1)	0.0169(7)	0.0176(5)	0.0167(7)	0.0177(8)	0.0184(7)
	<i>U</i> ₃₃	0.0117(7)	0.012(2)	0.0140(8)	0.0120(7)	0.0120(5)	0.0123(7)	0.0124(7)	0.0122(6)
	<i>U</i> ₁₂	0.0087(6)	0.010(2)	0.015(1)	0.0102(6)	0.0106(4)	0.0098(6)	0.0102(7)	0.0105(6)
	<i>U</i> ₁₃	-0.0037(6)	-0.003(2)	-0.002(1)	-0.0036(6)	-0.0028(4)	-0.0030(6)	-0.0034(7)	-0.0020(5)
	<i>U</i> ₂₃	-0.0049(6)	-0.005(2)	-0.002(1)	-0.0048(6)	-0.0049(4)	-0.0048(6)	-0.0054(8)	-0.0041(5)

Note: Standard deviations are in parentheses. The displacement parameters are of the form $\exp[-2\pi^2(U_{11}h^2a^2 + U_{22}k^2b^2 + U_{33}l^2c^2 + 2U_{12}hka^*b^* + 2U_{13}hla^*c^* + 2U_{23}kib^*c^*)]$. The isotropic temperature factor equivalents (*B*_{eq}) were calculated according to Hamilton (1959); the standard deviation of *B*_{eq} was estimated according to Schomaker and Marsh (1983).

TABLE 5. Cation distributions in osumilites obtained by site-occupancy refinements

Site name	Number of positions	Occupancy model	Antarctica	Norway	Eifel B93	Eifel Nickenich	Japan Shimizu	Japan Hayasaki	Sardinia	Oregon
C	1	K (K + Na + Ca)	0.91(1)	0.90(1)	0.48(1)	0.69(1)	0.74(1)	0.76(1)	0.75(1)	0.69(1)
		Vacancy	0.09	0.10	0.52	0.31	0.26	0.24	0.25	0.31
A	2	Fe (Fe + Mn + Ti)	0.02(2)	0.32(4)	1.34(2)	0.02(2)	1.12(2)	1.16(2)	0.82(2)	1.02(2)
		Mg (Mg + Al)	1.98	1.68	0.66	1.98	0.88	0.84	1.18	0.98
T2	3	Fe (Fe + Mn + Ti)	0.03(3)	0.09(3)	0.24(3)	0.24(3)	0.18(3)	0.21(3)	0.18(3)	0.18(3)
		Al (Al + Mg)	2.997	2.91	2.76	2.76	2.82	2.79	2.82	2.82
T1	12	Si (Si + Al)	12	12	12	12	12	12	12	12

Note: Element symbols in parentheses indicate elements that were simulated by the preceding element outside the parentheses. Numbers in parentheses are standard deviations as obtained in the site-occupancy refinements.

is tested in Figure 4 where the refined population of Fe in octahedral coordination is plotted versus the A–O distance. All samples but one show increasing A–O distances with increasing Fe occupation on A. However, the most Fe-rich crystal from the Eifel district (Eifel B93) shows the smallest A–O distance. Microprobe analyses in Table 1 and by Schreyer et al. (1983) indicate that, at least for this osumilite, Al in combination with Fe and Mg must be assumed to be in octahedral coordination; thus, the large size of Fe²⁺ is balanced by the small size of Al (Shannon, 1976: ^{VI}Fe²⁺, 0.78 Å; ^{VI}Al: 0.535 Å), so as to decrease the overall A–O distance.

The low alkali concentration for the osumilite Eifel B93 is related to the substitution ^{VI}Al³⁺ + ^{XII}vacancy =

^{VI}(Mg,Fe²⁺) + ^{XII}(K,Na). This replacement mechanism is also evident (Fig. 5) from the individual microprobe analyses of samples described in this paper and the average analyses on Eifel osumilites by Schreyer et al. (1983). Linear-regression analysis yields the relationship $Al(T2,A) = 3.35 - 0.666(K + Na)$, $R^2 = 81\%$ (51 observations), where the Al concentration on T2 and A is calculated as $Al_{tot} - (12 - Si)$. The linear regression suggests an alkali-free osumilite end member with the composition $^{A,T2}(Al_{3.35}(Mg,Fe^{2+})_{1.65})^{T1}(Si_{10.6}Al_{1.4})O_{30}$. A synthetic alkali-free osumilite-type phase with the assumed formula $^{A,T2}(Al_3Mg_2)^{T1}(Si_{11}Al)O_{30}$ has been identified by Schreyer and Schairer (1962).

Site-occupancy refinements for sample Eifel B93 yield-

TABLE 6. Selected interatomic distances and angles

	Antarctica	Norway	Eifel B93	Eifel Nickenich	Japan Shimizu	Japan Hayasaki	Sardinia	Oregon
C–O1 (12×)	3.099(2)	3.141(8)	3.120(4)	3.100(3)	3.099(2)	3.096(2)	3.097(3)	3.115(2)
A (Mg,Fe,Al) octahedron								
A–O3 (6×)	2.118(2)	2.128(5)	2.100(3)	2.110(2)	2.151(2)	2.154(2)	2.142(2)	2.145(2)
O3–O3 (3×)	2.553(3)	2.544(8)	2.542(5)	2.560(3)	2.579(2)	2.577(3)	2.577(3)	2.568(3)
O3–O3 (3×)	2.964(3)	2.991(9)	2.945(5)	2.951(3)	2.987(2)	2.992(3)	2.980(4)	2.982(3)
O3–O3 (6×)	3.219(2)	3.238(7)	3.185(4)	3.200(2)	3.285(2)	3.288(2)	3.262(4)	3.277(3)
Ti (Si,Al) tetrahedron								
T1–O1	1.6197(7)	1.616(2)	1.617(1)	1.6171(9)	1.6185(7)	1.6182(9)	1.618(1)	1.6208(8)
T1–O2	1.625(4)	1.622(12)	1.622(7)	1.620(4)	1.621(3)	1.624(4)	1.622(4)	1.620(4)
T1–O2	1.635(3)	1.658(8)	1.626(4)	1.628(3)	1.630(2)	1.629(3)	1.628(3)	1.630(3)
T1–O3	1.630(2)	1.621(4)	1.638(4)	1.627(2)	1.632(1)	1.635(2)	1.629(2)	1.636(2)
O1–T1–O2	111.4(2)	110.9(6)	111.3(3)	111.1(2)	111.3(1)	111.3(2)	111.2(2)	111.3(2)
O1–T1–O3	111.3(1)	111.7(3)	111.0(2)	111.3(2)	110.9(1)	110.9(1)	111.0(1)	110.9(1)
O1–T1–O2	112.1(2)	112.2(5)	112.2(3)	111.9(2)	111.6(2)	111.9(1)	111.6(3)	111.7(2)
O2–T1–O3	110.1(1)	109.1(4)	109.5(2)	110.1(1)	110.4(1)	110.4(1)	110.5(1)	110.0(1)
O2–T1–O2	105.6(1)	108.1(3)	107.9(2)	106.3(1)	106.0(1)	105.9(1)	105.9(1)	106.9(1)
O3–T1–O2	105.9(1)	104.6(4)	104.7(2)	106.0(1)	106.3(1)	106.2(4)	106.3(2)	105.8(1)
T2 (Al,Mg,Fe) tetrahedron								
T2–O3 (4×)	1.767(3)	1.756(9)	1.772(5)	1.775(3)	1.766(2)	1.764(3)	1.769(3)	1.762(3)
O3–O3 (2×)	2.553(3)	2.544(8)	2.542(5)	2.560(3)	2.579(2)	2.577(3)	2.577(3)	2.568(3)
O3–O3 (2×)	2.889(3)	2.862(8)	2.905(5)	2.906(3)	2.888(2)	2.885(3)	2.893(3)	2.884(3)
O3–O3 (2×)	3.178(2)	3.162(6)	3.198(3)	3.195(2)	3.155(2)	3.153(2)	3.168(2)	3.152(2)
O3–T2–O3 (2×)	92.5(1)	92.8(3)	91.6(2)	92.3(1)	93.81(7)	93.8(1)	93.5(1)	93.5(1)
O3–T2–O3 (2×)	109.7(1)	109.2(3)	110.1(2)	109.9(1)	109.75(8)	109.7(1)	109.7(1)	109.8(1)
O3–T2–O3 (2×)	128.2(1)	128.5(2)	128.9(1)	128.33(7)	126.56(4)	126.63(7)	127.08(7)	126.80(6)
T1–O1–T1	145.2(2)	145.7(5)	145.0(3)	145.6(2)	145.3(1)	145.3(2)	145.5(2)	144.5(1)
T1–O2–T1	153.3(1)	153.8(3)	153.8(2)	153.8(1)	154.0(1)	153.7(1)	153.9(1)	154.4(1)
T1–O3–T2	124.3(1)	124.8(2)	123.9(1)	124.0(1)	125.05(6)	125.07(8)	124.8(1)	125.0(2)

Note: Standard deviations are in parentheses.

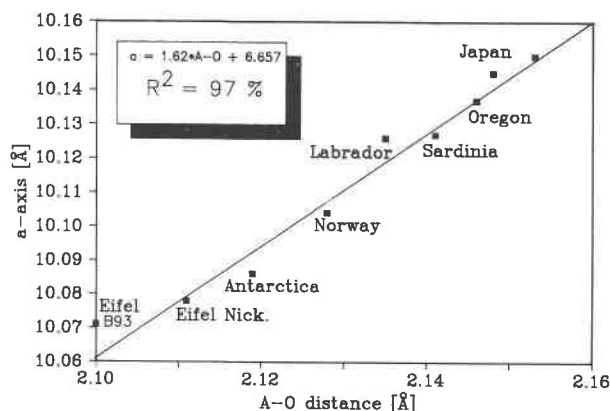


Fig. 3. The length of the *a* edge of the unit cell plotted vs. the A–O distance, as obtained from structure refinements. Data of the Labrador osumilite were adopted from Hesse and Seifert (1982); all other results are from this study.

ed 8% Fe on T2 (Table 5). If we neglect possible Mg on T2, this position (multiplicity 3) is occupied by 2.76 Al and 0.24 Fe (Table 5). Applying the above regression equation with the refined K concentration of 0.48, the positions A (multiplicity 2) and T2 (multiplicity 3) contain 3.03 Al. With 2.76 Al on T2, 0.27 Al remain for A. Site-occupancy refinements (Table 5) indicate 1.34 Fe on A; thus, an additional 0.39 Mg is assumed on this site. The predominant valence of Fe can be tested for this simplified cation distribution model by considering the following reference distances. The A–O distance for 100% Mg in A is 2.115 Å (Fig. 4), whereas for 100% Fe²⁺, it is 2.17 Å (extrapolated from Fig. 4). A value of A–O = 1.903 Å for 100% Al is derived from the beryl structure (Gibbs et al., 1968), and a value of 1.972 Å for predominantly Fe³⁺ in A is observed for the double-ring silicate sugilite (Arnbruster and Oberhänsli, 1988). Using these references, 67% Fe²⁺ in A leads to a mean A–O bond length of 2.123 Å for the Eifel B93 osumilite, whereas 67% Fe³⁺ would lead to 1.990 Å. The observed value of 2.100 Å suggests that predominantly Fe²⁺ occupies the A octahedron.

It is striking that site-occupancy refinements (allowing for Fe and Mg) yielded for all samples lower transition-metal concentrations⁵ on T2 and A than the microprobe analyses indicate for total Fe + Mn + Ti.⁶ This discrepancy might suggest that transition metals are not confined to T2 and A but are to a small degree distributed over other potential atomic positions. Mössbauer (Goldman and Rossman, 1978) and EXAFS experiments (Waychunas et al., 1986) confirm Fe in a disordered channel position. The (Fe,Mg) deficit on A could be balanced by excess Na. Replacement of Mg by Na in the A octahedron has been previously observed in the double-ring silicate eifelite (Abraham et al., 1983).

⁵ Small amounts of Mn and Ti cannot be distinguished from Fe by their X-ray scattering behavior.

⁶ Microprobe analyses were collected on different grains.

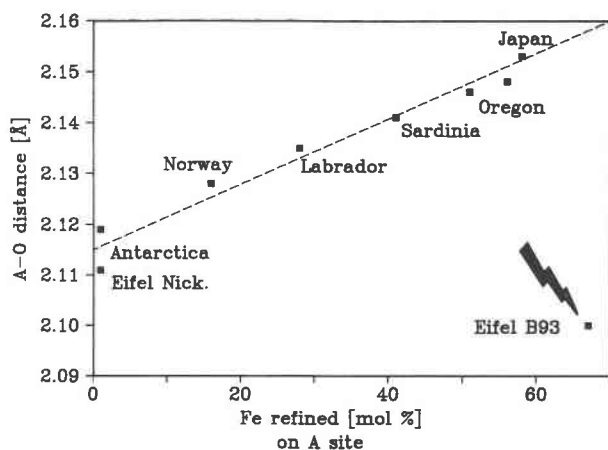


Fig. 4. All samples except the Eifel B93 osumilite show a linear correlation when the refined site occupancy of heavy metals (Fe) in A is plotted vs. the A–O distance. The high Fe content in this sample is compensated by octahedral Al; thus, the A–O distance does not increase.

The T2 tetrahedron

The T2 tetrahedron shares two edges with A octahedra (Fig. 1). As indicated previously, with increasing Fe, A–O distances increase. If the A octahedron expands, how does this increase affect the attached T2 tetrahedron?

Regression analyses indicate no significant correlation between A–O and T2–O distances nor between the Fe population in A and that in T2. Figure 6 shows an A octahedron surrounded by three edge-sharing T2 tetrahedra viewed along the *c* axis. All corners of the A octahedron and T2 tetrahedron are formed by O3-type oxygen atoms. Increase of A–O leads to an expansion of the

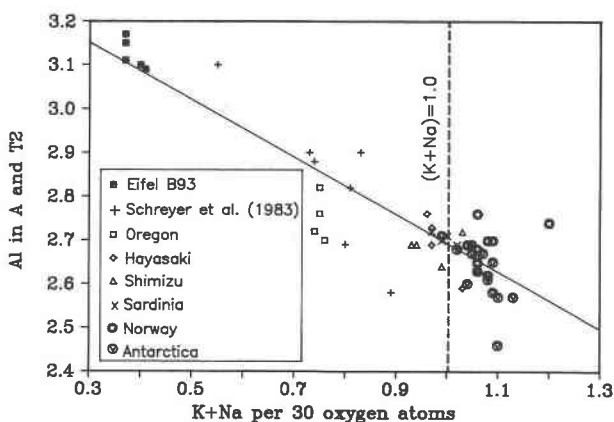


Fig. 5. Correlation between (K + Na) with Al in A and T2 per formula unit (30 oxygen atoms). The Al concentration in A and T2 is calculated as $Al_{tot} - (12 - Si)$. The linear-regression line supports the substitution mechanism $^{IV,VI}Al + ^{XII}vacancy = ^{IV,VI}(Mg, Fe^{2+}) + ^{XII}Na$. Cross symbols represent average analyses of Schreyer et al. (1983) on Eifel osumilites, whereas all other symbols represent individual microprobe analyses of samples described in this paper.

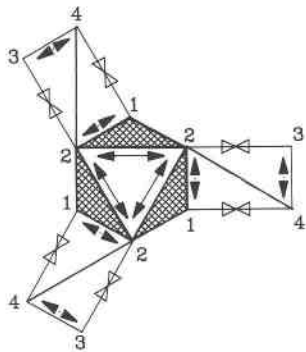


Fig. 6. The A octahedron linked to three strongly distorted edge-sharing T2 tetrahedra projected along the *c* axis. All corners of the polyhedra are formed by O3 oxygen atoms. The labels 1, 2, 3, and 4 of O3-type oxygen atoms are used for better description in the text. Filled arrows indicate expansion of O–O distances with increasing size of the cation centering the octahedron. Open arrows indicate shortening of O–O distances. The strongest increase of oxygen distances is observed in the triangles formed by those O3 atoms labeled 1 on the lower side and 2 on the upper side of the octahedron.

triangle formed by oxygen atoms labeled 2 on the upper and 1 on the lower side of the octahedron (Fig. 6). This expansion parallel to (001) is also responsible for the increase of *a* with A–O length. A slight increase of O–O distances with increasing A–O is also observed for the shared edge (oxygen atoms numbered 1,2 and 3,4). Simultaneously, the tetrahedral edges labeled 2,3 and 1,4 shorten (Fig. 6), which is the reason why the size of the T2 tetrahedron appears independent of the A–O distance.

The mean T2–O distance, 1.766 Å indicates this position to be dominated by Al³⁺. Site-occupancy refinements also yield low Fe concentrations of between 1 and 8%. The similarity between Al and Mg concerning their scattering behavior for X-rays does not allow one to draw conclusions about possible low Mg concentrations on T2 from site-occupancy refinements. However, the similarly coordinated T11 position in low cordierite, which is a pure Al site, exhibits a mean T11–O distance of ca. 1.752 Å (Armbruster, 1985), suggesting only minor amounts of Mg on the osumilite T2 site. The double-ring silicate merrihueite possesses only Mg on T2 leading to a T2–O distance of 1.955 Å (Kahn et al., 1972). Judging from the T2–O bond lengths in osumilites, the concentration of (Mg + Fe + Mn) is below 10% in T2, equivalent to 0.30 (Mg + Fe + Mn) per formula unit.

The T1 tetrahedron

With a mean T1–O distance ranging between 1.623 and 1.629 Å, the T1 tetrahedron, forming the six-membered double rings, is preferentially occupied by Si. Microprobe analyses (Table 1) indicate that in all crystals investigated, T1 is occupied by ca. 85% Si and additional Al. O3-type oxygen atoms connect the double rings (Fig. 1) with T2 and A. O3-type oxygen atoms labeled 2 and 4 (Fig. 6) belong to the upper double rings with their centers at

$z = 0$, while the oxygen atoms numbered 1 and 3 belong to the lower rings with their centers at $z = 0.5$ (Figs. 1, 6). If the distance between O3(1) and O3(2) is equal to the distance between O3(2) and O3(3), the double rings stacked above each other are rotated exactly 30° with respect to one another.

The cage position C

The population of the C site (Table 5) obtained from site-occupancy refinements allowing for K and vacancies probably does not reflect the true occupation, because Na is neglected. As a rule of thumb, for this type of X-ray site-occupancy refinement, one K combined with one vacancy might equate to two Na atoms (Na, 11 electrons; K, 19 electrons). Schreyer et al. (1983) showed on the basis of microprobe analyses of various osumilites that (K + Na + Ca) is smaller for osumilites formed under low pressure than for high-pressure osumilites. This result is confirmed by our measurements (Fig. 5). Site-occupancy refinements of osumilites from metamorphic terranes (Antarctica and Norway) show also the highest population on C, whereas the occupation is much lower for crystals of volcanic origin (Table 5). It is surprising that there is no significant correlation between the C–O distance and the population of C. Consequently, the displacement parameters (temperature factors) along the bonding vector C–O1 are independent of the population of C.

Although structure data and microprobe analyses were not collected on the same crystals, there are some striking relations: except for crystal Eifel B93, the refined K concentration (Table 5) obtained from site-occupancy refinements (allowing for K and vacancies) agrees fairly well with the K contents found by electron microprobe (Table 1). The average analysis of Schreyer et al. (1983) for Eifel B93 (their BIII) compared to ours (Table 1) from the same hand specimen indicates that for this type of osumilite, strong K variation is observed. The close correspondence between site occupancies and analytical K concentrations could suggest that most Na does not occupy the C position.

Other possible atomic sites: Facts and suppositions

In eifelite (Na₂KMg₂Al₃Si₁₂O₃₀), an osumilite-related double-ring silicate, the ¹⁸B' site is occupied by Na (Abraham et al., 1983). However, in structure refinements of osumilites (Brown and Gibbs, 1969; Hesse and Seifert, 1982) ¹⁸B or ¹⁸B' were hitherto not considered. When inspecting Figure 5, it is striking that almost half of the individual microprobe analyses yield (K + Na) sums above 1.0. Almost all high (K + Na) analyses belong to osumilites from metamorphic terranes, which agrees with the compilation of osumilite analyses by Schreyer et al. (1983; their Fig. 6). Thus, high (K + Na) values should not be discussed as analytical errors. The Antarctica osumilite proved to be fairly homogeneous; thus, for this sample, microprobe analyses can be compared with the refined site occupancies. Only 0.91 K could be located by

the structure refinement (Table 5), whereas average microprobe analyses yielded 1.08 (K + Na) (Table 1). Even if some Na completes the A site (microprobe analyses gave 4.96 cations, which were assigned to A and T2), the site for the excess alkalis is still uncertain.

The reader is reminded that Mössbauer investigations of Goldman and Rossman (1978) and EXAFS studies by Waychunas et al. (1986) on osumilites indicate that some of the Fe^{2+} is highly dispersed over various cage positions. However, before considering those poorly defined sites for alkalis in osumilites, some details about detection limits in single-crystal X-ray techniques applied in this and similar papers will be discussed. The noise level in difference-Fourier sections of the osumilites studied is about $\pm 0.5 \text{ e}/\text{\AA}^3$ with exception of the Norwegian crystal with $\pm 1 \text{ e}/\text{\AA}^3$. This background noise is mainly caused by insufficiencies of the model applied, e.g., neglect of anisotropic extinction, inadequate absorption correction, incomplete data collection, and scattering by bonding electrons or highly dispersed atoms. In cordierites (space group *Cccm*), full occupancy of the channel position 0,0,0 (site symmetry $2/m$) by Na would cause a maximum electron density in difference-Fourier sections of ca. $24 \text{ e}/\text{\AA}^3$ at 0,0,0 (Armbuster, 1986). 0.05 Na at 0,0,0 would still cause a peak above an assumed noise level of $\pm 0.5 \text{ e}/\text{\AA}^3$. However, if Na would be slightly disordered along the *c* axis on a position of the type 0,0,*z* (site symmetry 2), the occupancy factor splits and is only 0.025. The corresponding peaks in the difference-Fourier sections would be in the range of the noise level and could hardly be resolved. If these detection limits are transferred to osumilites, it follows that neither ^{18}B nor $^{xviii}\text{D}$ in the osumilites studied are occupied by more than ca. 0.03 atoms with an atomic weight similar to Na. Abraham et al. (1983) reported that Na in eifelite is slightly displaced from ^{18}B and occupies a $^{18}\text{B}'$ site at $1/3, 2/3, 0.019$. In the case of osumilites, such a disorder of minor Na concentrations would further increase the detection limit. Thus, X-ray single-crystal structure refinements like the ones presented here cannot determine over which positions small amounts of atoms are distributed.

OPTICAL PROPERTIES

The best single-variable model to describe the refractive indices (excluding sample Eifel B93 with octahedral Al) was obtained (Fig. 7) with the refined Fe population in octahedral coordination, P_{Fe} (calculated in mole percent), as independent variable: $\epsilon = 1.5435 + 0.00017P_{\text{Fe}}$, $R^2 = 95\%$; $\omega = 1.5315 + 0.00026P_{\text{Fe}}$, $R^2 = 97\%$. The Fe content, calculated as the sum of the populations of Fe in T2 and A, yielded a significantly poorer correlation. In addition, the refined K concentration on C did not significantly improve the model. Because of the difficulty in measuring the refractive indices parallel to *O* (see experimental section), higher-order models were not tried. As seen in Figure 7, osumilites rich in octahedral Mg possess the highest birefringence and are optically positive. With increasing Fe \leftrightarrow Mg substitution, ω increases more strongly

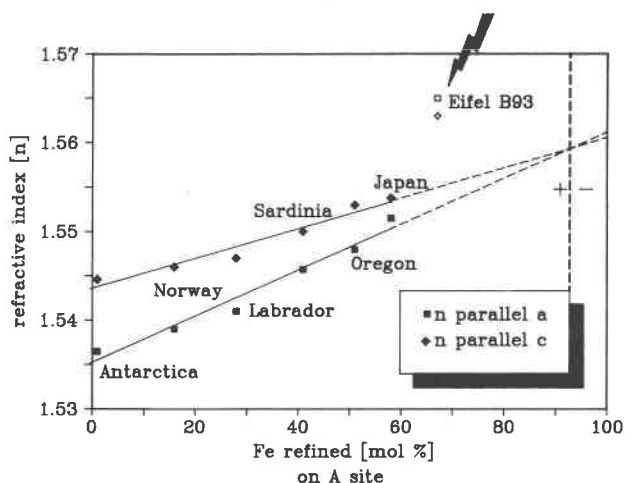


Fig. 7. The refined Fe population on the A octahedron is plotted vs. refractive indices. The birefringence decreases with increasing Fe content. Extrapolation to high Fe concentrations indicates that near 90% Fe, ϵ becomes equal to ω and the optic character changes from positive to negative. The octahedral Al-bearing Eifel (B93) osumilite does not follow this trend, but reveals higher refractive indices and is optically negative.

than ϵ , thus reducing the birefringence. Linear extrapolation to high Fe \leftrightarrow Mg substitution yields an isotropic crossover point at about 90% Fe on A. For higher octahedral Fe concentrations, osumilites are thus predicted to become optically negative.

The exception, sample Eifel B93 (Fig. 7) with octahedral Al, has significantly higher refractive indices. This sample has optically negative character and reveals only low birefringence. It is unclear whether it is a coincidence that the refined Fe content in A also correlates with the macroscopic color of osumilite: low-Fe samples (Antarctica, Eifel Nickenich) are colorless, medium-Fe osumilites (Norway, Labrador) are pink, and the high-Fe crystals are dark blue (Sardinia, Oregon, Eifel B93, Japan).

CONCLUSIONS

1. The length of the *a* axis of osumilites is strongly dependent on the A–O distance and the major cations in A (Fe, Mg, Al). The correlation of the *c*-axis length and the A–O distance is less pronounced.
2. The octahedrally coordinated A position is predominantly occupied by Mg and Fe^{2+} . However, one sample contains substantial amounts of Al on A.
3. The concentration of alkalis in osumilites is correlated with the concentration of Al replacing Mg and/or Fe^{2+} : $^{vi}\text{Al} + ^{xiii}\text{vacancy} = ^{vi}(\text{Mg}, \text{Fe}^{2+}) + ^{xii}(\text{K}, \text{Na})$.
4. Not all alkalis and bivalent cations found by electron-microprobe analyses could be assigned to specific sites in the structure refinements. It is assumed that some cations are distributed over additional sites.
5. For osumilites with predominantly Fe^{2+} and Mg on the A position, refractive indices increase with increasing

Fe content. In addition, ω increases more strongly than ϵ ; thus, a crossover point at about 90% Fe on A results where osumilites should have isotropic behavior. Low-Fe osumilites are optically positive. Extrapolation of refractive indices to high Fe concentrations suggests that osumilites with more than 90% Fe on A are optically negative.

6. One osumilite with partial substitution of the type ${}^{\text{VI}}\text{Al} + {}^{\text{XII}}\text{vacancy} \leftrightarrow {}^{\text{VI}}(\text{Mg,Fe}) + {}^{\text{XII}}(\text{K,Na})$ is optically negative and has higher refractive indices than corresponding Al-poor varieties.

ACKNOWLEDGMENTS

The sample Antarctica 2337K was kindly provided by E. Grew (Orono, Maine), sample Eifel B93 was donated by G. Hentschel (Wiesbaden, F.R.G.), and crystals from Cava Funtanafigu, Sardinia, Italy, were received from R. Hochleitner (München, F.R.G.). The Oregon, U.S.A. (no. A8491), Shimizu, Japan (no. A8458), and Eifel, Nickenich, F.R.G. (no. B343), osumilites are catalogued in the collection of the Museum of Natural History, Bern, and were made available to us by H. A. Stalder. An early version of this manuscript benefited from the reviews of B. Dutrow and R. Welsch. The reviews and thoughtful comments of W. Schreyer and F. D. Bloss are much appreciated. This study was supported by the Swiss "National Fonds."

All materials investigated are deposited at the mineralogy collection of the Museum of Natural History, Bernastr. 5, CH-3005 Bern, Switzerland. Sample numbers cited in this paper are museum numbers.

REFERENCES CITED

- Abraham, K., Gebert, W., Medenbach, O., Schreyer, W., and Hentschel, G. (1983) Eifelite, $\text{KNa}_3\text{Mg}_4\text{Si}_2\text{O}_{30}$, a new mineral of the osumilite group with octahedral sodium. *Contributions to Mineralogy and Petrology*, 82, 252–258.
- Arnbruster, Th. (1985) Fe-rich cordierites from acid volcanic rocks, an optical and X-ray single-crystal structure study. *Contributions to Mineralogy and Petrology*, 91, 180–187.
- (1986) Role of Na in the structure of low-cordierite: A single-crystal X-ray study. *American Mineralogist*, 71, 746–757.
- Arnbruster, Th., and Oberhänsli, R. (1988) Crystal chemistry of double-ring silicates: Structures of sugilite and brannockite. *American Mineralogist*, 73, 595–600.
- Bakakin, V.V., Ryllov, G.M., and Belov, N.V. (1970) X-ray diffraction data for identification of beryl isomorphs. *Geokhimiya*, 11, 1302–1311 (in Russian).
- Becker, P.J., and Coppens, P. (1974) Extinction within the limit of validity of the Darwin transfer equations. I. General formalisms for primary and secondary extinction and their application to spherical crystals. *Acta Crystallographica*, A30, 129–147.
- Berg, J.H., and Wheeler, E.P. (1976) Osumilite of deep-seated origin in the contact aureole of the anorthositic Nain complex, Labrador. *American Mineralogist*, 61, 29–37.
- Bloss, F.D. (1981) *The spindle stage, principles and practice*. Cambridge University Press, Cambridge.
- Brown, G.E., and Gibbs, G.V. (1969) Refinement of the crystal structure of osumilite. *American Mineralogist*, 54, 101–116.
- Enraf Nonius. (1983) Structure determination package (SDP). Enraf Nonius, Delft, Holland.
- Forbes, W.C., Baur, W., and Kahn, A.A. (1972) Crystal chemistry of milarite-type minerals. *American Mineralogist*, 57, 463–472.
- Gibbs, G.V., Breck, D.W., and Meagher, E.P. (1968) Structural refinement of hydrous and anhydrous synthetic beryl, $\text{Al}_2(\text{Be}_2\text{Si}_6)\text{O}_{18}$ and emerald, $\text{Al}_19\text{Cr}_{0.1}(\text{Be}_3\text{Si}_6)\text{O}_{18}$. *Lithos*, 1, 275–285.
- Goldman, D.S., and Rossman, G.R. (1978) The site distribution of iron and anomalous biaxiality in osumilite. *American Mineralogist*, 63, 490–498.
- Grew, E.S. (1982) Osumilite in the sapphirine-quartz terrane of Enderby Land, Antarctica: Implications for osumilite petrogenesis in granulite facies. *American Mineralogist*, 67, 762–787.
- Hamilton, W.C. (1959) On the isotropic temperature factor equivalent to a given anisotropic temperature factor. *Acta Crystallographica*, 12, 609–610.
- Hesse, K.F., and Seifert, F. (1982) Site-occupancy refinement of osumilite. *Zeitschrift für Kristallographie*, 160, 172–186.
- Hochleitner, R. (1982) Osumilith: Osumilith-Kristalle von der Cava Funtanafigu. *Lapis*, 7, nr. 11, 26–27.
- Kahn, A.A., Baur, W.H., and Forbes, W.C. (1972) Synthetic magnesian merrihueite, dipotassium pentamagnesium dodecasilicate: A tetrahedral magnesian silicate framework crystal structure. *Acta Crystallographica*, B28, 267–272.
- Majjer, C., Hansen, J.B.H., Wevers, J., and Poorter, R.P.E. (1977) Osumilite, a mineral new to Norway. *Norsk Geologisk Tidsskrift*, 57, 187–188.
- Miyashiro, A. (1956) Osumilite, a new silicate mineral, and its crystal structure. *American Mineralogist*, 41, 104–116.
- Olesch, M., and Seifert, F. (1981) The restricted stability of osumilite under hydrous conditions in the system $\text{K}_2\text{O-MgO-Al}_2\text{O}_3\text{-SiO}_2\text{-H}_2\text{O}$. *Contributions to Mineralogy and Petrology*, 76, 362–367.
- Olsen, E., and Bunch, T.E. (1970) Composition of natural osumilites. *American Mineralogist*, 55, 875–879.
- Schomaker, V., and Marsh, R.E. (1983) On evaluating the standard deviation of U_{eq} . *Acta Crystallographica*, A39, 819–820.
- Schreyer, W., and Schairer, J.F. (1962) Metastable osumilite- and petalite-type phases in the system $\text{MgO-Al}_2\text{O}_3\text{-SiO}_2$. *American Mineralogist*, 47, 90–104.
- Schreyer, W., Hentschel, G., and Abraham, K. (1983) Osumilith in der Eifel und die Verwendung dieses Minerals als petrogenetischer Indikator. *Tschermak's Mineralogische und Petrographische Mitteilungen*, 32, 215–234.
- Schreyer, W., Blümel, P., and Maresch, W. (1986) Cordierit und Osumilith aus den Buchiten der Blauen Kuppe bei Eschwege. *Aufschluss*, 37, 353–367.
- Selkregg, K.R., and Bloss, F.D. (1980) Cordierites: Compositional controls of Δ , cell parameters, and optical properties. *American Mineralogist*, 65, 522–533.
- Shannon, R.D. (1976) Revised effective ionic radii and systematic studies of interatomic distances in halides and chalcogenides. *Acta Crystallographica*, A32, 751–767.
- Waychunas, G.A., Brown, G.E., and Apter, M.J. (1986) X-ray K-edge absorption spectra of Fe minerals and model compounds: II. EXAFS. *Physics and Chemistry of Minerals*, 13, 31–47.
- Zucker, U.H., Perenthaler, E., Kuhs, W.F., Bachmann, W.F., and Schulz, H. (1983) PROMETHEUS, a program system for investigation of anharmonic vibrations in crystals. *Journal of Applied Crystallography*, 16, 358.

MANUSCRIPT RECEIVED JULY 24, 1987

MANUSCRIPT ACCEPTED JANUARY 8, 1988